Journal of Alloys and Compounds 897 (2022) 163113

Contents lists available at ScienceDirect

Journal of Alloys and Compounds

journal homepage: www.elsevier.com/locate/jalcom

Atomic layer deposition-based synthesis of TiO_2 and Al_2O_3 thin-film coatings on nanoparticle powders for sodium-ion batteries with enhanced cyclic stability

Song Yeul Lee[1], Dasom Park[1], Byung Sun Yoon, Yun-Sung Lee*, Yong Il Park*, Chang Hyun Ko*

School of Chemical Engineering, Chonnam National University, Gwangju 61186, Republic of Korea

ARTICLE INFO

Article history:
Received 1 August 2021
Received in revised form 14 October 2021
Accepted 2 December 2021
Available online 4 December 2021

Keywords:
Atomic layer deposition
Sodium-ion batteries
Energy storage
Electrode materials
Protective layer
Thin films

ABSTRACT

Despite it being the leading technology for fabricating uniform-thickness metal and metal-oxide thin films on wafer-based substrates, atomic layer deposition (ALD) is yet to be utilized with powder-based substrates. Via the successful deposition of TiO_2 and Al_2O_3 thin films on the surfaces of silica (SiO_2) nanospheres, Prussian blue (PB) nanocubes, and $NaTi_2(PO_4)_3$ (NTP) nanocubes using a home-built ALD system, this study demonstrates that ALD is a viable technique for depositing thin films on powdered substrates. Furthermore, amorphous TiO_2 thin films are used as a protective layer to enhance the electrochemical properties of NTP nanocubes, which have application prospects in sodium-ion batteries. Whereas uncoated NTP nanocubes loses 67.9% of its initial charge capacity within 100 charge/discharge cycles, TiO_2-coated (thickness: ~ 3 nm) NTP nanocubes reduces this capacity loss to 22.1%. This strongly suggests that powder-optimized ALD can be used to fabricate thin films for multiple applications that use powder-type nanoparticles, such as electrode materials and catalysts.

1. Introduction

Lithium-ion batteries (LIBs) are a key component of energy storage systems used for multiple purposes; in particular, with the development of electric vehicles, their demand is increasing. However, with its reserves being limited, lithium is becoming an increasingly expensive commodity. Recently, the low price of sodium has seen sodium-ion (Na^+) batteries (SIBs) thrust into the spotlight as an alternative to LIBs for energy storage systems [1–3]. In addition, sodium reserves are abundant, and the electrochemical characteristics of Na^+ are similar to those of Li^+ [4–7]. However, since relatively large size of Na^+ affects the volume change of the electrode material during charging and discharging, SIBs are hindered by their low cyclic stability over long periods of use [8]. To solve this problem, several studies have reported on potential electrode material developments such as new methods for electrode material synthesis [9], composite formation [10], and coating surfaces [11–13]. Among these approaches, surface coating techniques have proven to be the most effective strategy for improving the cyclic stability of conventional electrode materials. Typically, coating of surfaces using carbon or metal oxides is performed using a liquid-phase synthetic method; however, the range of suitable coating materials is limited depending on the electrode material, and achieving coatings with a uniform thickness is challenging [14]. Previous studies on the fabrication of semiconductor devices have demonstrated that gas-phase coating can solve the difficulties encountered in liquid-phase coating [15]. Gas-phase surface coating methods include chemical vapor deposition (CVD), whereby coating layers are formed via chemical reactions, and physical vapor deposition (PVD), whereby coating layers are formed via recondensation as the deposited vapor cools. Neither of these coating methods offers surface conformality or the ability to control the coating thickness at the nanoscale. Furthermore, volatile precursors are prone to generating impurities owing to incomplete decomposition. Atomic layer deposition (ALD), a type of CVD that deposits materials in single-atom layers, does not suffer from such problems. Because ALD applies the precursors in sequence, only a single layer of atoms is deposited per cycle, thus facilitating precise thickness control. Further, as the single-atom layers are deposited via adsorption, they adhere to the surface effectively, irrespective of location, and are conformal. In addition, there are far fewer restrictions regarding material selection [16–19]. Owing to these advantages, ALD is widely deployed in the semiconductor industry and in the production of energy storage systems. However,

* Corresponding authors.
E-mail addresses: leeys@jnu.ac.kr (Y.-S. Lee), ypark@jnu.ac.kr (Y. Il Park), chko@jnu.ac.kr (C.H. Ko).
[1] These authors are equally contributed.

https://doi.org/10.1016/j.jallcom.2021.163113
0925-8388/

because conventional ALD is designed to work with wafer-based substrates, it is seldom utilized for coating nanoparticles. Although both fluidized beds and rotary reactors have been developed for this purpose, high precursor losses during the reaction means that they are extremely inefficient [20], while there is a risk of leakage during rotation, which leads to the aggregation of powders owing to the high operating temperature [21]. The use of protective coatings on the surfaces of coin-cell-type electrodes using wafer-based ALD has also been explored as a means of improving the performance of battery electrodes [22–24]. However, as these coin cells consist of a mixture of conductive materials and binders, there is a risk of decomposition when performing ALD at high temperatures. Therefore, it is necessary to use ALD to coat electrode materials in the powdered form [14]. To this end, we have developed a home-built batch-type ALD instrument that uses precursors efficiently and can form uniform-thickness thin films on the surface of powdered nanomaterials. Using the proposed ALD system, TiO_2 and Al_2O_3 thin films were successfully deposited on the surface of powder-type nanoparticles including $NaTi_2(PO_4)_3$ (NTP) nanocubes, silica (SiO_2) nanospheres, and Prussian blue (PB) nanocubes. A SIB using optimally coated NTP nanocubes as the anode material maintained its initial charging capacity after repeated charge/discharge cycles for considerably longer than uncoated NTP nanocubes, demonstrating that the proposed batch-type ALD method is a useful and viable approach for applying thin-film coatings on powder-type nanoparticles.

2. Experimental procedure

2.1. Synthesis of nanoparticles

SiO_2 nanospheres were synthesized using the Stöber method [25]. First, 10 mL of NH_4OH was added to a 40 mL solution of ethanol and distilled water (mixed in a ratio of 3:2 by volume) and stirred for 30 min (solution A). Next, 5 mL of tetraethyl orthosilicate was mixed in 45 mL of ethanol (solution B). Then, solutions A and B were combined and stirred at room temperature for 5 h. The product was recovered via centrifugation and washed several times with distilled water and ethanol. Finally, it was dried in an oven at 80 °C overnight.

The PB nanocubes were prepared according to the procedure reported in [26]. First, 4 mmol of sodium ferrocyanide was added to 200 mL of distilled water, and the temperature was raised to 60 °C. Next, 2 mmol of HCl solution (37%) was added to the solution, which was stirred for 4 h while maintaining the temperature at 60 °C. The PB nanocubes were collected via centrifugation, washed with distilled water and ethanol, and dried in an oven at 80 °C overnight.

The NTP nanocubes were synthesized using a hydrothermal method [27]. First, 4 g of anatase TiO_2, 4 g of NaH_2PO_4, 4 mL of distilled water, and 4 mL of H_3PO_4 were mixed using a pestle and mortar. This mixture was placed in a 200 mL Teflon-lined autoclave and heated at 150 °C for 6 h. The resulting particles were collected via centrifugation, rinsed several times with distilled water, and dried in an oven at 80 °C overnight.

To increase the electrochemical conductivity of TiO_2-coated NTP, the surface of each sample was further modified with a carbon layer. NTP nanocubes and TiO_2-coated NTP were dispersed in oleic acid overnight. The samples were collected by centrifugation and calcined at 800 °C for 2 h under Ar.

2.2. ALD procedure

To deposit the Al_2O_3 and TiO_2 thin films, we constructed a batch-type ALD reactor (see Fig. S1). The home-built ALD instrument consists of a vacuum pump, a trap, and three chambers, two of which are for precursors and the other for the powdered material being coated (e.g., NTP nanocubes, SiO_2 nanospheres, and PB nanocubes). To coat a uniform thin film on powder-type nanomaterials by ALD, precursor molecules should be adsorbed as a monolayer on high-surface-area nanomaterial powder. This requires a higher partial pressure of the precursor and a longer precursor contacting time. The home-built ALD instrument developed in this study achieves these requirements and simply coats thin films on powder-type nanomaterials. Proper valve operation and evacuation allow powdered nanomaterials and precursor molecules to coexist in the same closed space. In that space, the precursor molecules achieve a higher partial pressure of the precursor as the only gas-phase component. Therefore, they easily diffuse into the voids between the nanomaterials. It is also easy to achieve longer precursor contacting time by simply maintain the valve position fixed. In contrast, it is very difficult to achieve these conditions with conventional flow-type ALD instrument. Because conventional instrument was designed based on fixed-bed reactor, most of the precursor molecules may be wasted due to the short contacting time, and a longer precursor contacting time may only be achieved by increasing the precursor feeding time and flow rate. Nevertheless, conventional instrument limits the maximum partial pressure of the precursor because an inert gas (N_2 or Ar) carries the precursor molecules towards the nanomaterial powder. Therefore, considering the working mechanism and advantages, the home-built batch-type ALD instrument developed in this study is suitable for uniformly coating TiO_2 and Al_2O_3 thin films on nanomaterial powders.

The base vacuum pressure of the ALD reactor was maintained at approximately 0.05 mbar (0.038 torr). Prior to coating, the chamber containing the precursor was subjected to freeze-vacuum-thaw degassing to remove gaseous impurities other than the precursor. To ensure that they were coated uniformly and received maximum exposure to the precursor gases, only a small amount (250 mg) of the powder-type nanoparticles were used.

For the TiO_2 coating, titanium isopropoxide (TTIP, > 97%, Sigma Aldrich) and deionized (DI) water were used as precursors. To increase the vapor pressure of TTIP to 12 mmHg, the TTIP reservoir was heated to 80 °C. The DI water was not heated because the room-temperature vapor pressure was sufficient. The tube connecting the precursor reservoirs and the powder material reservoir was heated to 80 °C to prevent the precursor gases from condensing. In addition, the nanoparticles were heated to 250 °C, which is the maximum temperature at which TTIP does not decompose, to guarantee a sufficient level of adsorption and reaction. The temperature of the powder chamber was maintained at 250 °C during the ALD process. In the designed ALD system, one cycle of ALD comprises four steps. First (step 1), gas-phase TTIP was supplied to the powder chamber for 600 s to saturate the TTIP vapor. Next (step 2), the powder chamber was evacuated to remove the gas-phase and physically adsorbed TTIP. Then (step 3), water (in gas phase) was supplied to the powder chamber for 600 s to saturate the water vapor and convert TTIP into TiO_2. Finally (step 4), the powder chamber was evacuated for 600 s to remove the reaction products (isopropyl alcohol) and the unreacted water. The number of ALD cycles was determined to control the thickness of the TiO_2 thin film.

For the Al_2O_3 coating, aluminum isopropoxide (AIP, ≥ 98%, Sigma Aldrich) and DI water were used as precursors. To increase the vapor pressure of AIP to 1.33 mmHg, it was heated to 120 °C (the water was not heated for the reason mentioned earlier). The tube connecting the precursor reservoirs and the powder material reservoir was heated to 120 °C because the gas-phase precursor was not condensed. The powder-type nanoparticles were heated to 120 °C (AIP decomposes above this temperature) to ensure a sufficient level of

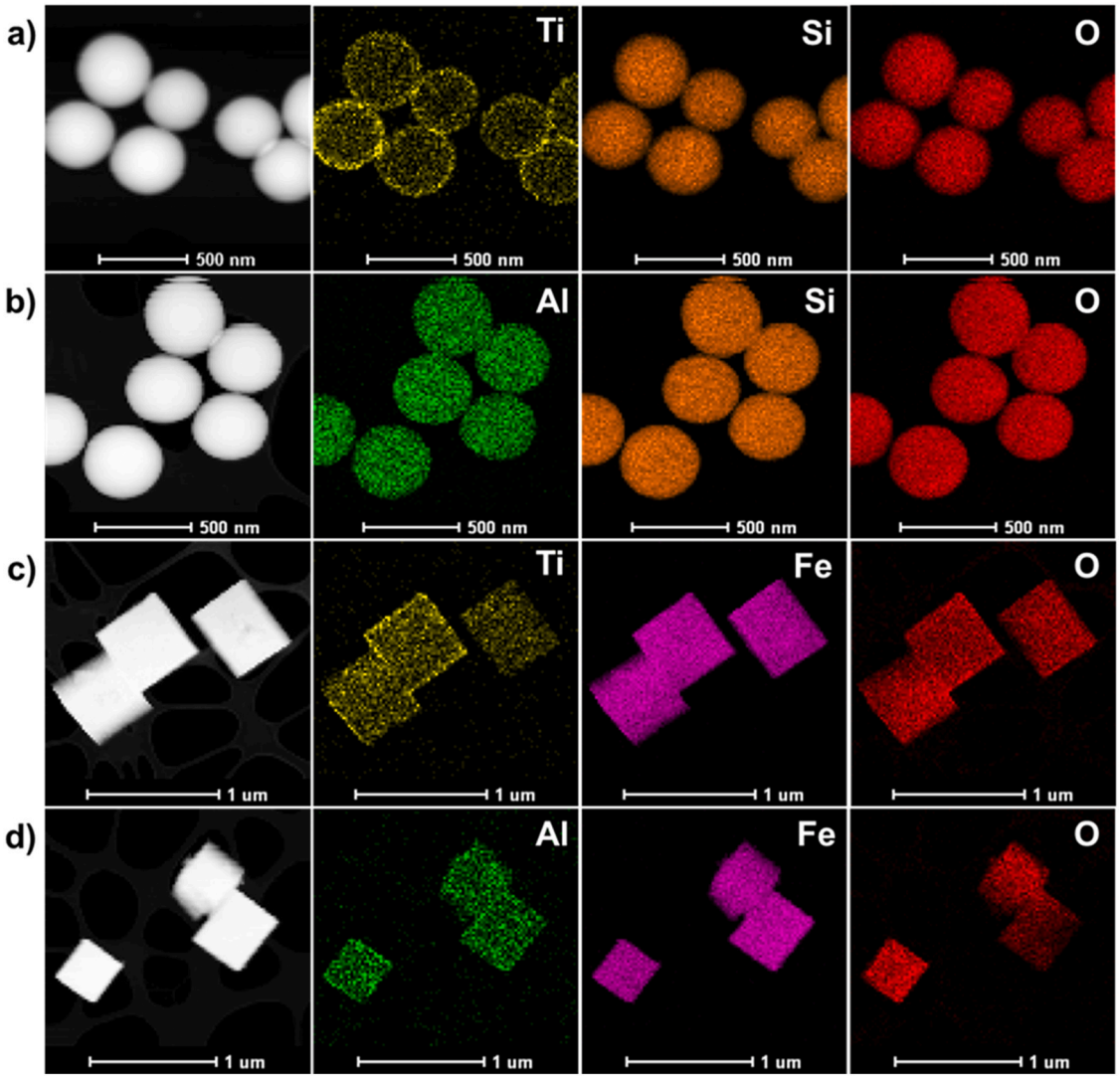

Fig. 1. Representative high-angle annular dark-field scanning transmission electron microscopy (HAADF-STEM) images and elemental maps for (a) TiO_2 thin films on SiO_2 nanospheres, (b) Al_2O_3 thin films on SiO_2 nanospheres, (c) TiO_2 thin films on PB nanocubes, and (d) Al_2O_3 thin films on PB nanocubes.

reaction. The coating procedure followed the same four steps, as described for TiO_2. Similarly, the number of ALD cycles was determined to control the thickness of Al_2O_3 thin film.

2.3. Characterization

The morphology of each material and the variation in the thickness of the TiO_2 and Al_2O_3 surface layers according to the number of ALD cycles were observed using transmission electron microscopy (TEM, JEOL 2010, Japan). The composition of the coating layers was confirmed via TEM-based element mapping (TECNAI G2 F20, USA). X-ray photoelectron spectroscopy (XPS, K-ALPHA+ spectrometer, USA) was used to analyze the relative concentrations of Ti and Al ions according to the number of ALD coatings. X-ray diffraction (XRD, Rigaku Rint 1000, Japan) was performed to analyze the changes in the crystal structure of the synthesized materials before and after being coated using the ALD system. The surface functional groups of the nanoparticles before and after the ALD coating process were confirmed via infrared spectroscopy analysis (IR, Shimadzu IR Prestige-21, Japan).

2.4. Electrochemical characterization

The electrodes were made by casting slurry comprising active material, carbon black, and polyvinylidene difluoride (PVDF) in a weight ratio of 7:2:1 on Al foil. The typical electrode mass loading ranged from 1.5 to 2.0 mg/cm^2. The electrochemical properties of the uncoated NTP nanocubes and the TiO_2-coated NTP nanocubes were measured using a CR2032 coin-type half-cell. The coin cells were assembled in an Ar-filled glovebox: a Na metal disk was used as the counter and reference electrodes, and the electrolyte comprised 1 M $NaClO_4$ in equal volumes of ethylene carbonate (EC) and dimethyl carbonate (DMC). Whatman glass fiber (GF/F) was used as the separator. The galvanostatic charge/discharge test and the cyclic performance were measured versus Na/Na^+ using a Won-A-Tech battery tester (WBCS 3000, Korea) in the 1.5–2.8 V voltage range. The

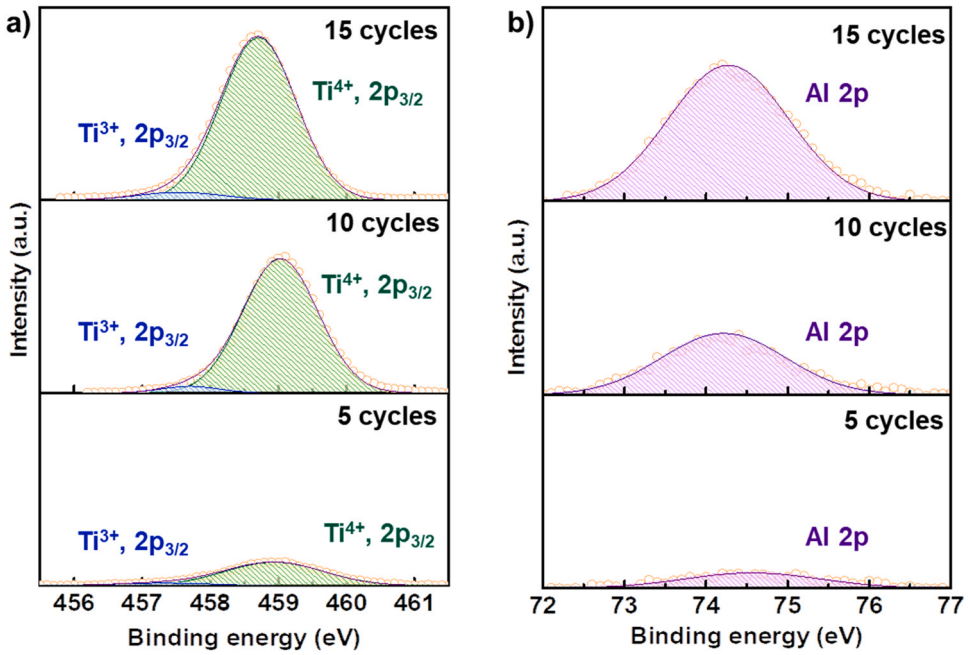

Fig. 2. XPS spectra of the TiO_2 and Al_2O_3 films deposited on SiO_2 nanospheres: (a) Ti 2p spectra, (b) Al 2p spectra.

Table 1
Atomic % of Ti in the TiO_2 thin films on the SiO_2 nanospheres.

Cycle No.	0	5	10	15
Ti atomic %	0.00	1.80	10.76	12.89

Table 2
Atomic % of Al in the Al_2O_3 thin films on the SiO_2 nanospheres.

Cycle No.	0	5	10	15
Al atomic %	0.00	1.03	2.04	7.40

electrochemical impedance spectroscopy (EIS) measurements were performed versus Na/Na^+ using Won-A-Tech impedance tester (SP1, Korea) at various scan rates in the 1.5–2.8 V voltage range.

3. Results and discussion

The uniformity of the ALD-fabricated thin-film coatings was verified using uniform nanoparticles such as SiO_2 nanospheres and PB nanocubes. After performing 10 ALD cycles to synthesize TiO_2 and Al_2O_3 coatings on the surfaces of the SiO_2 nanospheres and PB nanocubes, elemental maps were obtained using HAADF-STEM. Fig. 1a and c show TiO_2-coated SiO_2 nanospheres and PB nanocubes, respectively. Although it is faint because of the small amount of material used, the TiO_2 is uniformly coated on the exterior of the SiO_2 nanospheres. In contrast, Fig. 1(b) and (d) show the Al_2O_3-coated SiO_2 nanospheres and PB nanocubes, respectively. After 10 ALD coating cycles, the amount of Al deposited is comparable to the amount of Ti deposited during the TiO_2 deposition.

The TiO_2 and Al_2O_3 coatings were deposited on SiO_2 nanospheres via 5, 10, and 15 ALD cycles, with XPS analysis performed to measure the respective Ti and Al concentrations. Fig. 2a and Table 1 show that the atomic % of Ti increases as the number of TiO_2 deposition cycles increases. A similar trend is observed for Al_2O_3, with Fig. 2b and Table 2 showing that the % of Al atoms increases as the number of Al_2O_3 deposition cycles increases. However, whereas the atomic % of TiO_2 increases most rapidly when the number of ALD cycles increases from 5 to 10, for Al_2O_3, the largest increase occurs when the number of ALD cycles increases from 10 to 15. Considering the penetration depth of XPS, the non-linearity of the Ti and Al concentrations can be ascribed to the XPS analysis only measuring the concentrations within the topmost 10 nm of the coatings rather than the total concentrations throughout the samples.

The interfaces between the coatings (TiO_2 or Al_2O_3) and the SiO_2 nanosphere surfaces cannot be distinguished clearly via TEM owing to their amorphous structure. In addition, the PB nanocubes are crystalline but very thick, making the lattice pattern difficult to verify via TEM. Conversely, the crystalline NTP nanocubes are well-defined (Fig. S2), allowing the thicknesses of the ALD-synthesized TiO_2 and Al_2O_3 thin films to be confirmed using TEM. As a consequence, the NTP nanocubes were selected for further stability testing to determine their suitability for SIBs. As NTP is an electrode material whose cyclic stability decreases during long-term charging and discharging, its cyclic stability is expected to increase when it is coated with a protective layer of optimal thickness. To determine the optimal thickness, TiO_2 thin films were deposited on the surfaces of NTP nanocubes, with the changes in thickness according to the number of ALD cycles measured through TEM analysis. Fig. 3a, b, and c show TEM images of TiO_2-coated NTP following 10, 20, and 30 cycles of ALD, respectively. The TEM images show that the thickness of the amorphous TiO_2 thin film deposited on the crystalline NTP lattice increases as the number of ALD cycles increases. The relationship between the thickness of the TiO_2 coating and the number of cycles is shown in Fig. 3d, with the plotted data and the error bars representing the mean ± standard deviation of three measurements. As the number of ALD cycles increases, the thickness increases linearly: the equation of the trend line is $y = 0.2335x - 0.1162$, which corresponds to an increase of approximately 2.3 Å per cycle. The deposition rate for ALD-synthesized TiO_2 thin films has been reported as 1.2 Å per cycle at 100 °C [28]. However, the deposition rate observed here exceeds that value. To clarify this, we repeated the TiO_2 thin-film coating process with the NTP nanocubes and the feeding time maintained (600 s), while the heating temperature of target material chamber was lowered to 100 °C. The corresponding TEM image is shown in Fig. S3. Lowering the temperature to 100 °C

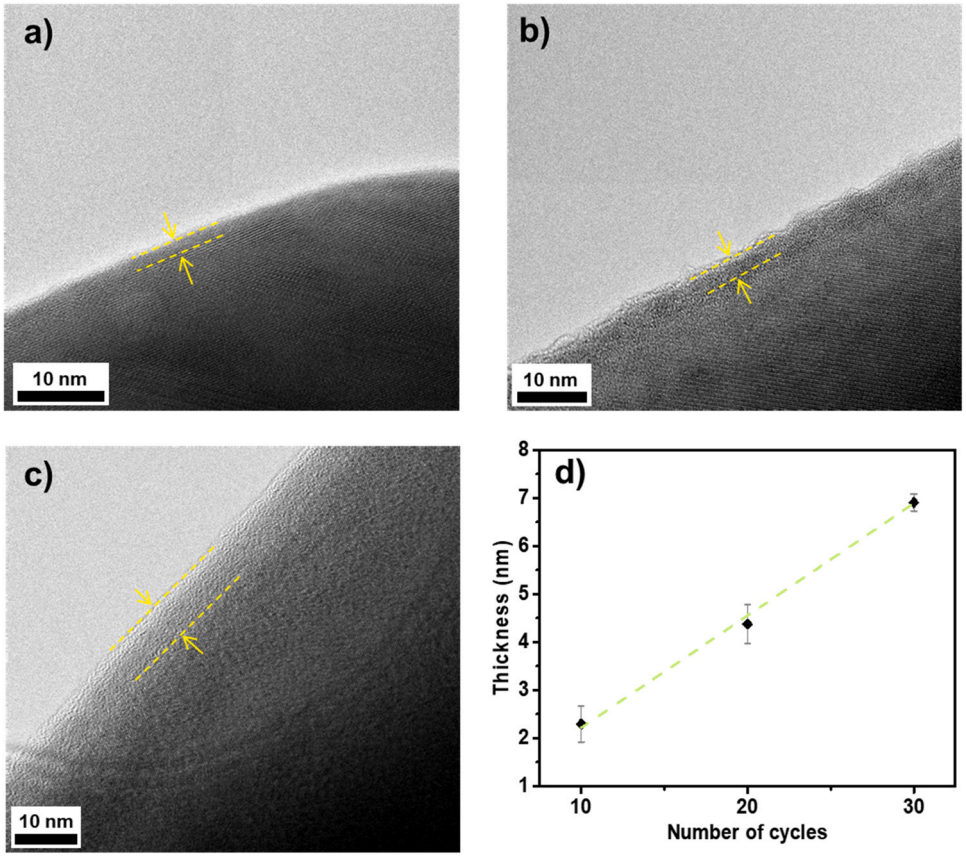

Fig. 3. TEM images of TiO_2 films deposited on the NTP lattice at 250 °C: (a) 10 cycles, (b) 20 cycles, (c) 30 cycles, and (d) coating thickness as a function of the number of ALD cycles.

resulted in the deposition rate falling to 1.6 Å per cycle, which is closer to the value reported in [20]. Therefore, the ALD mode is dominant when coating is performed at 100 °C. At 250 °C, the coating temperature approaches the decomposition temperature of TTIP, and therefore, the ALD is supplemented by CVD when forming the TiO_2 thin films on the surface of the NTP nanocubes.

A similar tendency was observed for the Al_2O_3 thin films. Fig. 4 shows the evolution in film thickness as a function of the number of ALD cycles. As with the TiO_2 thin films, the thickness of the non-crystalline Al_2O_3 thin films increases linearly as the number of cycles increases: the equation of this trend line is $y = 0.1312x + 0.3649$, corresponding to a deposition rate of approximately 1.3 Å per cycle. This Al_2O_3 deposition rate is consistent with values reported elsewhere [29,30], indicating that the ALD was conducted under favorable conditions [31,32]. Note that aluminum isopropoxide (AIP) was used as the precursor of Al_2O_3 and not trimethylaluminum (TMA). Typically, the highly reactive TMA is considered to produce better-quality Al_2O_3 thin films than AIP when using ALD [33,34]. However, we successfully realized the ALD of uniform-thickness Al_2O_3 coatings using AIP, which is a safer precursor.

The electrochemical performances of TiO_2-coated NTP nanocubes produced using several different numbers of ALD cycles were evaluated using a half-cell with Na metal serving as the counter and reference electrodes. Fig. 5a shows the galvanostatic charge/discharge curves of the samples for four different TiO_2 coating thicknesses, with the measurements performed between 1.5 V and 2.8 V with a current density of 100 mA/g. The plateaus at 2.1 V and 2.2 V correspond to the Ti^{4+}/Ti^{3+} redox reactions induced by sodiation and desodiation, respectively (Fig. 5a and Fig. S4) [35]. The initial capacity increased after 5 cycles of ALD coating, which can be explained by the synergistic effect between the surface layer and the active material, and prevention of solid electrolyte interphase (SEI) film formation [36,37]. To confirm the improvement that the ALD coatings make to the electrochemical properties of the test battery, the pristine sample was not subjected to additional heat treatment, which resulted in large polarization between the plateaus of the pristine cube. This polarization is reduced by coating the pristine cube with amorphous TiO_2 because the electrolyte infiltrates the amorphous shell, reducing the migration distance of Na^+ ions and resulting in rapid ion exchange between the interfaces [38]. As the coating thickness increases with the number of ALD cycles, the slope of the plateau gradually increases because Na^+ ions are sequentially inserted/extracted through the amorphous TiO_2. In addition, the passive layer established by the ALD coating stabilizes or prevents the formation of a SEI layer, while the flexibility of the amorphous structure increases the structural stability by reducing the volume change due to the charge/discharge process, demonstrating that this characteristic is effective for improving the cyclic stability of the battery [39,40]. The cyclic performance of all samples was evaluated at the same current density (Fig. 5b). Increasing the thickness of the ALD-fabricated coating enhanced the battery stability without causing a sharp deterioration in its specific capacity. Notably, uncoated NTP retains only 32.1% of its initial capacity after 100 charge/discharge cycles, while 77.9% remains when the NTP nanocubes are coated using 15 ALD applications of TiO_2. As the number of ALD cycles increases, the charge/discharge cycle stability of the NTP nanocubes was improved, but the initial capacity was decreased (Fig. S5).

EIS was performed with a symmetrical cell and the results were fitted by the ZMAN program (Fig. 5c). The semicircle at high frequency can be ascribed to the charge transfer resistance (R_{ct}). Compared with NTP nanocubes, the size of the semicircle increases as the ALD cycles increases, and the resistance increases sharply at 15 ALD cycles, due to the increase in TiO_2 film thickness. To further

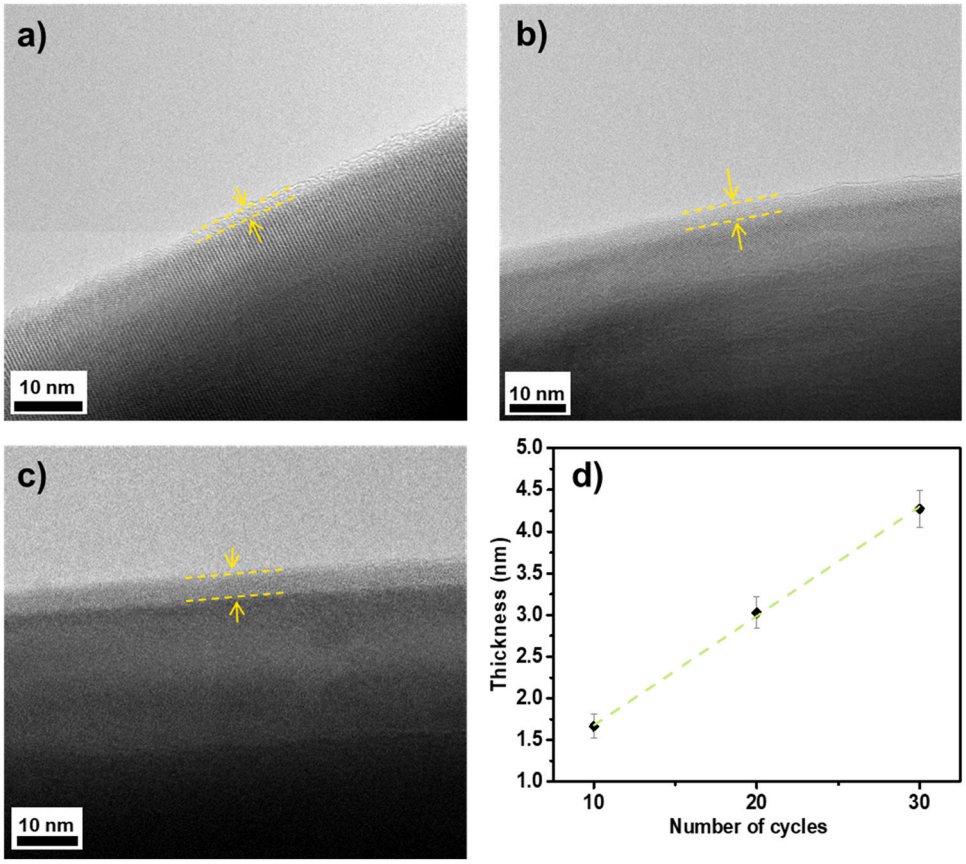

Fig. 4. TEM images of Al_2O_3 films deposited on the NTP lattice: (a) 10 cycles, (b) 20 cycles, (c) 30 cycles, and (d) coating thickness as a function of the number of ALD cycles.

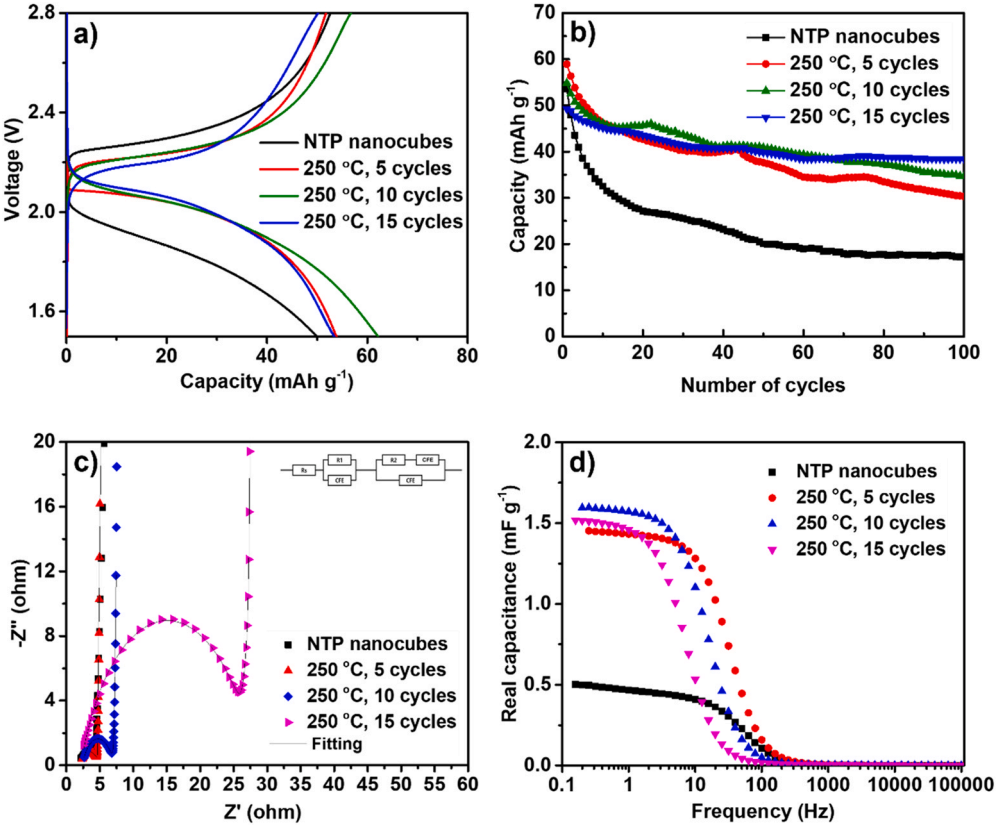

Fig. 5. (a) Charge/discharge curves for TiO_2-coated NTP nanocubes produced using different numbers of ALD cycles. (b) Cyclic stability of TiO_2-coated NTP nanocubes as a function of the number of cycles. (c) Nyquist plots and (c) plots of real capacitance against frequency for TiO_2-coated NTP nanocubes produced using different numbers of ALD cycles.

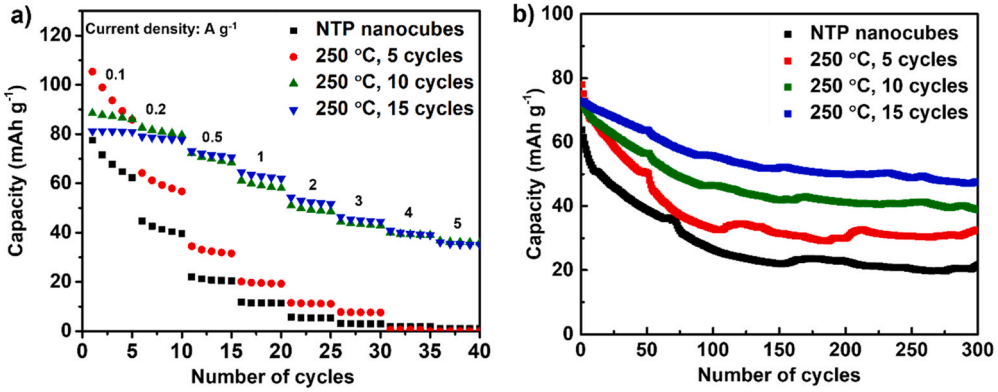

Fig. 6. (a) Rate performance of the carbon-coated NTP@TiO_2. (b) Cyclic stability of the carbon-coated NTP@TiO_2 at a current density of 0.2 A g^{-1}.

investigate of ion diffusivity, the real capacitance was plotted against frequency (Fig. 5d). The real capacitance (C′) was calculated using following equation:

$$C'(\omega) = \frac{-Z''(\omega)}{\omega\,|Z(\omega)|^2}$$

where Z″ is the imaginary impedance (ohm), ω is the frequency (Hz), and Z is the complex impedance (ohm). In the frequency region around 100 Hz, the C′ value starts to increase because ions accumulate on the electrode surface. When 5 ALD cycles were performed, the ionic diffusivity was higher compared to the pristine NTP nanocubes because the C″ value began to increase at higher frequency [41]. This may explain why the sample with 5 ALD cycles has a higher initial capacity. The samples with 10 ALD cycles and 15 ALD cycles samples had reduced ionic diffusivity due to the increased TiO_2 film thickness.

Due to the low electrical conductivity of NTP coated with amorphous TiO_2, the samples showed overall low electrochemical performance. Therefore, the surface of NTP@TiO_2 was modified with carbon to improve the electrochemical performance (Fig. S6). Surface modification with carbon increased the capacity of TiO_2-coated NTP nanocubes (Fig. 6a). And, with increasing current density, NTP nanocubes and samples with 5 ALD cycles showed a sharp decrease in capacity. However, the samples with the 10 ALD cycles and 15 ALD cycles showed relatively high capacity retention, which is considered to be due to the structural and electrochemical stability of the thick TiO_2 layer. The cyclic stability of carbon modified samples was measured at a current density of 0.2 A g^{-1} (Fig. 6b). The initial capacity of the pristine NTP nanocubes was 78.8 mA h g^{-1}, leaving only 26.6% of the initial capacity after 300 cycles. In contrast, the NTP@TiO_2 with 15 ALD cycles showed an initial capacity of 78.0 mA h g^{-1} and retention of 66.0% after 300 cycles. After cycling, the nanostructure did not collapse, and the structure was maintained (Fig. S7). However, at high current density, only the sample with 15 ALD cycles showed a retention of about 62.1% of the initial capacity after 500 cycles, and the capacity of the samples with 5 ALD cycles and 10 ALD cycles decreased rapidly after the initial several cycles (Fig. S8). These results demonstrate that the proposed ALD system enables the uniform coating of powder-type nanoparticles, thereby improving the electrochemical performance of the encapsulated active material.

4. Conclusion

In summary, we developed a batch-type ALD instrument for applying uniform metal-oxide thin-film coatings to the surface of powder-type nanoparticles. To demonstrate the capabilities of the proposed ALD system, uniform-thickness TiO_2 and Al_2O_3 thin films were synthesized on the surfaces of several different powdered nanoparticles, namely NTP nanocubes, silica nanospheres, and PB nanocubes. The thin-film coatings serve as a protective layer that increases the cyclic stability of the electrode material. In particular, TiO_2-coated NTP nanocubes were used to fabricate a prototype SIB with substantially improved electrochemical properties. The TiO_2-coated NTP exhibited superior cyclic stability than that of uncoated NTP, indicating that the ALD-based coating of powder nanoparticles can be utilized to improve the performance of electrode materials and catalysts.

CRediT authorship contribution statement

Song Yeul Lee: Methodology, Validation, Formal analysis, Investigation, Writing – original draft, Writing – review & editing. **Dasom Park:** Methodology, Validation, Formal analysis, Investigation, Writing – original draft. **Byung Sun Yoon:** Investigation. **Yun-Sung Lee:** Conceptualization, Supervision, Project administration, Funding acquisition. **Yong Il Park:** Conceptualization, Validation, Writing – original draft, Writing – review & editing, Supervision, Project administration, Funding acquisition. **Chang Hyun Ko:** Conceptualization, Methodology, Validation, Writing – original draft, Writing – review & editing, Supervision, Project administration, Funding acquisition.

Declaration of Competing Interest

The authors declare that they have no known competing financial interests or personal relationships that could have appeared to influence the work reported in this paper.

Acknowledgments

This work was supported by National Research Foundation of Korea (NRF) grants funded by the Korean government (Ministry of Science, ICT & Future Planning) (No. 2019R1A4A2001527).

Appendix A. Supporting information

Supplementary data associated with this article can be found in the online version at doi:10.1016/j.jallcom.2021.163113.

References

[1] Q. Zhang, Y. Lu, W. Guo, Y. Shao, L. Liu, J. Lu, X. Rong, X. Han, H. Li, L. Chen, Y.-S. Hu, Hunting sodium dendrites in NASICON-based solid-state electrolytes, Energy Mater. Adv. 2021 (2021) 9870879, https://doi.org/10.34133/2021/9870879
[2] T. Sato, K. Yoshikawa, W. Zhao, T. Kobayashi, H.B. Rajendra, M. Yonemura, N. Yabuuchi, Efficient stabilization of Na storage reversibility by Ti integration into O′3-type $NaMnO_2$, Energy Mater. Adv. 2021 (2021) 9857563, https://doi.org/10.34133/2021/9857563

[3] N. Voronina, S.-T. Myung, Recent advances in electrode materials with anion redox chemistry for sodium-ion batteries, Energy Mater. Adv. 2021 (2021) 9819521, https://doi.org/10.34133/2021/9819521

[4] K. Chayambuka, G. Mulder, D.L. Danilov, P.H.L. Notten, Sodium-ion battery materials and electrochemical properties reviewed, Adv. Energy Mater. 8 (2018) 1800079, https://doi.org/10.1002/aenm.201800079

[5] N. Yabuuchi, K. Kubota, M. Dahbi, S. Komaba, Research development on sodium-ion batteries, Chem. Rev. 114 (2014) 11636–11682, https://doi.org/10.1021/cr500192f

[6] V. Palomares, P. Serras, I. Villaluenga, K.B. Hueso, J. Carretero-González, T. Rojo, Na-ion batteries, recent advances and present challenges to become low cost energy storage systems, Energy Environ. Sci. 5 (2012) 5884–5901, https://doi.org/10.1039/C2EE02781J

[7] S.-W. Kim, D.-H. Seo, X. Ma, G. Ceder, K. Kang, Electrode materials for rechargeable sodium-ion batteries: potential alternatives to current lithium-ion batteries, Adv. Energy Mater. 2 (2012) 710–721, https://doi.org/10.1002/aenm.201200026

[8] M. Lin, M. Deng, C. Zhou, Y. Shu, L. Yang, L. Ouyang, Q. Gao, M. Zhu, Popcorn derived carbon enhances the cyclic stability of MoS_2 as an anode material for sodium-ion batteries, Electrochim. Acta 309 (2019) 25–33, https://doi.org/10.1016/j.electacta.2019.04.070

[9] S. Zhu, Q. Li, Q. Wei, R. Sun, X. Liu, Q. An, L. Mai, $NiSe_2$ nanooctahedra as an anode material for high-rate and long-life sodium-ion battery, ACS Appl. Mater. Interfaces 9 (2017) 311–316, https://doi.org/10.1021/acsami.6b10143

[10] Y. Pan, X. Cheng, M. Gao, Y. Fu, J. Feng, L. Gong, H. Ahmed, H. Zhang, V.S. Battaglia, Cagelike $CoSe_2$@N-doped carbon aerogels with pseudocapacitive properties as advanced materials for sodium-ion batteries with excellent rate performance and cyclic stability, ACS Appl. Mater. Interfaces 12 (2020) 33621–33630, https://doi.org/10.1021/acsami.0c06296

[11] J.-J. Ding, Y.-N. Zhou, Q. Sun, Z.-W. Fu, Cycle performance improvement of $NaCrO_2$ cathode by carbon coating for sodium ion batteries, Electrochem. Commun. 22 (2012) 85–88, https://doi.org/10.1016/j.elecom.2012.06.001

[12] Y. Zhao, X. Cao, G. Fang, Y. Wang, H. Yang, S. Liang, A. Pan, G. Cao, Hierarchically carbon-coated $Na_3V_2(PO_4)_3$ nanoflakes for high-rate capability and ultralong cycle-life sodium ion batteries, Chem. Eng. J. 339 (2018) 162–169, https://doi.org/10.1016/j.cej.2018.01.088

[13] W. Ren, W. Zhou, H. Zhang, C. Cheng, ALD TiO_2-coated flower-like MoS_2 nanosheets on carbon cloth as sodium ion battery anode with enhanced cycling stability and rate capability, ACS Appl. Mater. Interfaces 9 (2017) 487–495, https://doi.org/10.1021/acsami.6b13179

[14] Y. Liu, X.-J. Lin, Y.-G. Sun, Y.-S. Xu, B.-B. Chang, C.-T. Liu, A.-M. Cao, L.-J. Wan, Precise surface engineering of cathode materials for improved stability of lithium-ion batteries, Small 15 (2019) 1901019, https://doi.org/10.1002/smll.201901019

[15] M. Knez, K. Nielsch, L. Niinistö, Synthesis and surface engineering of complex nanostructures by atomic layer deposition, Adv. Mater. 19 (2007) 3425–3438, https://doi.org/10.1002/adma.200700079

[16] T.M. Onn, L. Arroyo-Ramirez, M. Monai, T.-S. Oh, M. Talati, P. Fornasiero, R.J. Gorte, M.M. Khader, Modification of Pd/CeO_2 catalyst by atomic layer deposition of ZrO_2, Appl. Catal. B 197 (2016) 280–285, https://doi.org/10.1016/j.apcatb.2015.12.028

[17] T.M. Onn, M. Monai, S. Dai, L. Arroyo-Ramirez, S. Zhang, X. Pan, G.W. Graham, P. Fornasiero, R.J. Gorte, High-surface-area, iron-oxide films prepared by atomic layer deposition on γ-Al_2O_3, Appl. Catal. A 534 (2017) 70–77, https://doi.org/10.1016/j.apcata.2017.01.025

[18] T.M. Onn, S. Zhang, L. Arroyo-Ramirez, Y. Xia, C. Wang, X. Pan, G.W. Graham, R.J. Gorte, High-surface-area ceria prepared by ALD on Al_2O_3 support, Appl. Catal. B 201 (2017) 430–437, https://doi.org/10.1016/j.apcatb.2016.08.054

[19] C. Lin, J.B. Jang, L. Zhang, E.A. Stach, R.J. Gorte, Improved coking resistance of "intelligent" Ni catalysts prepared by atomic layer deposition, ACS Catal. 8 (2018) 7679–7687, https://doi.org/10.1021/acscatal.8b01598

[20] J.D. Ferguson, K.J. Buechler, A.W. Weimer, S.M. George, SnO_2 atomic layer deposition on ZrO_2 and Al nanoparticles: pathway to enhanced thermite materials, Powder Technol. 156 (2005) 154–163, https://doi.org/10.1016/j.powtec.2005.04.009

[21] L.F. Hakim, J.L. Portman, M.D. Casper, A.W. Weimer, Aggregation behavior of nanoparticles in fluidized beds, Powder Technol. 160 (2005) 149–160, https://doi.org/10.1016/j.powtec.2005.08.019

[22] Y.S. Jung, A.S. Cavanagh, A.C. Dillon, M.D. Groner, S.M. George, S.-H. Lee, Enhanced stability of $LiCoO_2$ cathodes in lithium-ion batteries using surface modification by atomic layer deposition, J. Electrochem. Soc. 157 (2010) A75, https://doi.org/10.1149/1.3258274

[23] Y.S. Jung, A.S. Cavanagh, L.A. Riley, S.-H. Kang, A.C. Dillon, M.D. Groner, S.M. George, S.-H. Lee, Ultrathin direct atomic layer deposition on composite electrodes for highly durable and safe Li-Ion batteries, Adv. Mater. 22 (2010) 2172–2176, https://doi.org/10.1002/adma.200903951

[24] J.W. Kim, J.J. Travis, E. Hu, K.-W. Nam, S.C. Kim, C.S. Kang, J.-H. Woo, X.-Q. Yang, S.M. George, K.H. Oh, S.-J. Cho, S.-H. Lee, Unexpected high power performance of atomic layer deposition coated $Li[Ni_{1/3}Mn_{1/3}Co_{1/3}]O_2$ cathodes, J. Power Sources 254 (2014) 190–197, https://doi.org/10.1016/j.jpowsour.2013.12.119

[25] W. Stöber, A. Fink, E. Bohn, Controlled growth of monodisperse silica spheres in the micron size range, J. Colloid Interface Sci. 26 (1968) 62–69, https://doi.org/10.1016/0021-9797(68)90272-5

[26] Y. You, X.-L. Wu, Y.-X. Yin, Y.-G. Guo, High-quality Prussian blue crystals as superior cathode materials for room-temperature sodium-ion batteries, Energy Environ. Sci. 7 (2014) 1643–1647, https://doi.org/10.1039/C3EE44004D

[27] J. Yang, H. Wang, P. Hu, J. Qi, L. Guo, L. Wang, A high-rate and ultralong-life sodium-ion battery based on $NaTi_2(PO_4)_3$ nanocubes with synergistic coating of carbon and rutile TiO_2, Small 11 (2015) 3744–3749, https://doi.org/10.1002/smll.201500144

[28] J. Aarik, A. Aidla, T. Uustare, M. Ritala, M. Leskelä, Titanium isopropoxide as a precursor for atomic layer deposition: characterization of titanium dioxide growth process, Appl. Surf. Sci. 161 (2000) 385–395, https://doi.org/10.1016/S0169-4332(00)00274-9

[29] M.D. Groner, F.H. Fabreguette, J.W. Elam, S.M. George, Low-temperature Al_2O_3 atomic layer deposition, Chem. Mater. 16 (2004) 639–645, https://doi.org/10.1021/cm0304546

[30] L. Henn-Lecordier, M. Anderle, E. Robertson, G.W. Rubloff, Impact of parasitic reactions on wafer-scale uniformity in water-based and ozone-based atomic layer deposition, J. Vac. Sci. Technol. A 29 (2011) 051509, https://doi.org/10.1116/1.3620421

[31] A.W. Ott, J.W. Klaus, J.M. Johnson, S.M. George, Al_2O_3 thin film growth on Si(100) using binary reaction sequence chemistry, Thin Solid Films 292 (1997) 135–144, https://doi.org/10.1016/S0040-6090(96)08934-1

[32] A.W. Ott, K.C. McCarley, J.W. Klaus, J.D. Way, S.M. George, Atomic layer controlled deposition of Al_2O_3 films using binary reaction sequence chemistry, Appl. Surf. Sci. 107 (1996) 128–136, https://doi.org/10.1016/S0169-4332(96)00503-X

[33] C.A. Wilson, R.K. Grubbs, S.M. George, Nucleation and growth during Al_2O_3 atomic layer deposition on polymers, Chem. Mater. 17 (2005) 5625–5634, https://doi.org/10.1021/cm050704d

[34] T. Weckman, K. Laasonen, First principles study of the atomic layer deposition of alumina by TMA–H_2O-process, PCCP 17 (2015) 17322–17334, https://doi.org/10.1039/C5CP01912E

[35] C. Wu, P. Kopold, Y.-L. Ding, P.A. van Aken, J. Maier, Y. Yu, Synthesizing porous $NaTi_2(PO_4)_3$ nanoparticles embedded in 3D graphene networks for high-rate and long cycle-life sodium electrodes, ACS Nano 9 (2015) 6610–6618, https://doi.org/10.1021/acsnano.5b02787

[36] Y. Bai, D. Yan, C. Yu, L. Cao, C. Wang, J. Zhang, H. Zhu, Y.-S. Hu, S. Dai, J. Lu, W. Zhang, Core-shell Si@TiO_2 nanosphere anode by atomic layer deposition for Li-ion batteries, J. Power Sources 308 (2016) 75–82, https://doi.org/10.1016/j.jpowsour.2016.01.049

[37] X. Zhang, I. Belharouak, L. Li, Y. Lei, J.W. Elam, A. Nie, X. Chen, R.S. Yassar, R.L. Axelbaum, Structural and electrochemical study of Al_2O_3 and TiO_2 coated $Li_{1.2}Ni_{0.13}Mn_{0.54}Co_{0.13}O_2$ cathode material using ALD, Adv. Energy Mater. 3 (2013) 1299–1307, https://doi.org/10.1002/aenm.201300269

[38] C. Liu, Z.G. Neale, G. Cao, Understanding electrochemical potentials of cathode materials in rechargeable batteries, Mater. Today 19 (2016) 109–123, https://doi.org/10.1016/j.mattod.2015.10.009

[39] Y. Fang, L. Xiao, J. Qian, X. Ai, H. Yang, Y. Cao, Mesoporous amorphous $FePO_4$ nanospheres as high-performance cathode material for sodium-ion batteries, Nano Lett. 14 (2014) 3539–3543, https://doi.org/10.1021/nl501152f

[40] Y. Yin, Y. Hu, P. Wu, H. Zhang, C. Cai, A graphene–amorphous $FePO_4$ hollow nanosphere hybrid as a cathode material for lithium ion batteries, Chem. Commun. 48 (2012) 2137–2139, https://doi.org/10.1039/C2CC17381F

[41] W. Kim, D. Jang, H.-J. Kim, Understanding electronic and Li-ion transport of $LiNi_{0.5}$Co0.2Mn0.3O2 electrodes affected by porosity and electrolytes using electrochemical impedance spectroscopy, J. Power Sources 510 (2021) 230338, https://doi.org/10.1016/j.jpowsour.2021.230338